Available online at www.sciencedirect.com
SCIENCE DIRECT®
ELSEVIER
International Journal of Solids and Structures 43 (2006) 828–841
INTERNATIONAL JOURNAL OF SOLIDS and STRUCTURES
www.elsevier.com/locate/ijsolstr

Thermal loading in multi-layered and/or functionally graded materials: Residual stress field, delamination, fatigue and related size effects

Alberto Carpinteri *, Nicola Pugno

Department of Structural Engineering and Geotechnics, Politecnico di Torino, Corso Duca degli Abruzzi 24, 10129 Torino, Italy

Received 13 October 2004; received in revised form 9 May 2005
Available online 27 July 2005

Abstract

The stress field and fracture propagation due to thermal loading in multi-layered and/or functionally graded composite materials are extensively analysed. Regarding fracture, we have focused the attention on delamination between the layers due to brittle or fatigue thermally induced crack propagations. The statically indeterminate stress analysis is solved coupling equilibrium, compatibility and constitutive equations. Fracture analysis is based on the classical Griffith's criterion rewritten for composite structures under thermal loading. As an example, a two-layer prismatic structure is considered, each layer being composed by a different functionally graded material. The solution is particularized for the case of a linear grading. The size and shape effects are discussed and an optimization procedure is proposed. A numerical application of the findings to hard metal and diamond based cutters concludes the paper.

Keywords: Thermal loading; Functionally graded materials; Residual stresses; Delamination; Size-effects

1. Introduction

The spatial variation of the physical properties of the materials is an attractive alternative to composite solids, opening new possibilities for optimizing both materials and structural components to achieve high performance and efficiency. Such materials are collectively referred to as functionally graded materials or FGMs. Gradual variation of material properties in FGMs, unlike abrupt changes encountered in discretely layered systems, is known to improve failure performance while preserving the intended thermal, tribological, and/or structural benefits of combining dissimilar materials. Consequently, the concept of using

* Corresponding author. Tel.: +39 11 564 4850; fax: +39 11 564 4899.
E-mail addresses: alberto.carpinteri@polito.it (A. Carpinteri), nicola.pugno@polito.it (N. Pugno).

0020-7683/$ - see front matter
doi:10.1016/j.ijsolstr.2005.05.009

FGMs, for improving material performance, has recently received considerable attention from the research community (Paulino, 2002). On the other hand, it also poses at the same time challenging mechanics problems including the understanding of stress distribution and fracture behavior. These open problems will be considered in the present paper.

Pioneer papers on fracture mechanics of FGMs were written by Atkinson and List (1978), Delale and Erdogan (1983) and Eischen (1987). They show that the asymptotic crack tip stress field presents the same square root singularity as that encountered in homogeneous materials. More recently, Erdogan (1995) propose the multiplication of the conventional stress at a given point in crack tip vicinity by the ratio of the Young's modulus evaluated at that point to the Young's modulus at the crack tip. This hypothesis satisfies the equations of compatibility exactly, although—being limited in its own region of dominance—it obviously does not satisfy the equilibrium conditions.

Extensive research on various aspects of fracture of isotropic FGMs has been recently conducted, not only under mechanical loads, as previously discussed, but also under thermal loads (Jin and Noda, 1993; Erdogan and Wu, 1996; Jin and Batra, 1996; Wang et al., 2000; Jin and Paulino, 2001; Wang and Noda, 2001), Mixed-Mode I, II (Eischen, 1987; Ozturk and Erdogan, 1997, 1999) and Mode III (Babaei and Lukasiewicz, 1998). Experimental investigations on fracture of FGMs are limited by the high costs of the facilities required for processing FGMs. Relatively fewer experimental and numerical investigations of the fracture behavior of FGMs have been conducted. Among the few experimental investigations on FGMs, Parameswaran and Shukla (1998) have shown that increasing toughness in the direction of crack growth reduces crack jump distance in discretely layered FGMs. The extension of the crack analysis to the more general case of a re-entrant corner (Carpinteri and Pugno, 2005) in FGMs has been recently proposed (Carpinteri et al., in press).

In this paper we focus the attention on the stress field and fracture propagation due to thermal loading in multi-layered and/or functionally graded composite materials. The related size and shape effects are also discussed. The statically indeterminate stress analysis is solved coupling equilibrium, compatibility and constitutive equations, and extending the approach already established for torsional loading on bi-component prismatic or cylindrical (Pugno, 1999, 2001; Pugno and Surace, 2000, 2001; Pugno and Carpinteri, 2002) beams in static or dynamic regime. Regarding fracture, the attention is posed on delamination between the layers due to brittle or fatigue thermally induced crack propagations. Fracture analysis is based on the classical Griffith's criterion rewritten for composite structures under thermal load. The same approach was successfully applied by Pugno and Carpinteri (2002) to study the crack propagation under mechanical loading in prismatic and cylindrical homogeneous adhesive joints. This analysis can be considered the natural extension to thermal loading and functionally graded materials of the research on axially loaded tubular structures (Pugno and Carpinteri, 2003). An example of application to hard metal and diamond based cutters (Lammer, 1988; Huang et al., 1997) concludes the paper.

2. Thermal stresses in FGMs

The problem of residual stresses (induced by hot bonding of two different layers) is equivalent, neglecting the algebraic sign, to the problem of thermal stresses induced by a temperature increase in an already bonded two-layer structural component. This principle can be summarized as $\Delta T + \text{bonding} \equiv \text{bonding} - \Delta T$. As a consequence, we could study the problem of residual stresses induced in a composite structure (Fig. 1) bonded at an increased temperature ΔT, as the problem of thermal stresses induced by a decreased temperature (minus) ΔT.

Let us consider the two-layered structural component reported in Fig. 1. The axial equilibrium along the longitudinal axis (x) provides the tangential stresses at the interface of the two layers (Fig. 1) (Pugno and Surace, 2001):

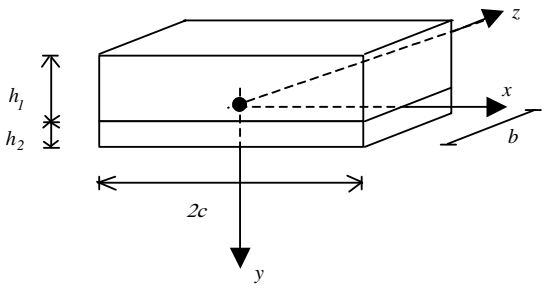

Fig. 1. Composite structure.

$$\tau(x) = -\frac{1}{b}\frac{\mathrm{d}N_1(x)}{\mathrm{d}x} \tag{1}$$

where $N_1(x)$ is the axial load in the first layer at a generic cross-section x and b is the width of the FGM structure.

Due to the axial equilibrium, the axial loads in a generic cross-section x can be written as

$$N_1(x) = N(x), \qquad N_2(x) = -N_1(x) = -N(x) \tag{2}$$

where $N_2(x)$ is the axial load in the second layer.

The sum of the forces absorbed by the two elements must be equal to zero. On the other hand, the rotational equilibrium suggests that the axial loads are applied at the interface level ($y = 0$). Satisfying the load boundary conditions implies that the axial load must be equal to zero at the extreme faces ($x = \mp c$, $2c$ being the length of the FGMS), as well as its first derivative must be equal to zero in the middle ($x = 0$) of the structure, due to the symmetry of the problem (Pugno and Surace, 2000; Pugno, 2001; Pugno and Carpinteri, 2003):

$$N(x = \pm c) = 0, \qquad \frac{\mathrm{d}N}{\mathrm{d}x}(x = 0) = 0 \tag{3}$$

Function $N(x)$, and thus the load absorbed by the two elements, can be found thanks to the displacement compatibility of the two elements at a given cross-section. The axial loads, being applied at the interface, result in stresses at the interface equal to $\frac{k_i N_i(x)}{A_i}$, where A_i is the cross-section area and k_i (a function of the grading) represents the ratio of the stress at the interface to its mean value $\frac{N_i(x)}{A_i}$. Accordingly, the displacements at the interface may be expressed as follows:

$$u_1(x, y = 0) = k_1 \int_0^x \frac{N(\xi)}{E_1 A_1}\,\mathrm{d}\xi - \alpha_1 \Delta T_1 x \tag{4a}$$

$$u_2(x, y = 0) = k_2 \int_0^x \frac{-N(\xi)}{E_2 A_2}\,\mathrm{d}\xi - \alpha_2 \Delta T_2 x \tag{4b}$$

where E_i is the Young's modulus, α_i the coefficient of thermal expansion and ΔT_i the increment in temperature, for the layer ith. The symmetry implies displacements equal to zero at $x = 0$. The algebraic signs—before ΔT_i—are due to our attention on residual stresses rather than on thermal ones.

For FGM α_i and E_i are dependent on y and must be evaluated at $y = 0$, in Eqs. (4). For varying cross-section area, A_i has to be considered as dependent on x. We herein consider constant cross-section areas.

The compatibility equation can be written noting how, after deformation, the relative displacement Δu between two points of the interface, can be evaluated as relative displacement between the two layers or as shearing deformation of the interface, its thickness h being very small, i.e. (Pugno and Surace, 2000; Pugno, 2001; Pugno and Carpinteri, 2003):

$$\Delta u(x) = u_2(x) - u_1(x) = h\gamma(x) = h\frac{\tau(x)}{G} \tag{5}$$

where G is the (mean) shear elastic modulus of the interface.

Substituting Eq. (1) into Eq. (5), the compatibility equation can be rewritten as

$$\frac{\mathrm{d}N(x)}{\mathrm{d}x} = -K^*\Delta u(x), \qquad K^* = \frac{Gb}{h} \tag{6}$$

where K^* is the interface stiffness per unit length.

Inserting the displacement expressions (4) in the compatibility equation (6), gives the following integral-differential equation in the unknown $N(x)$:

$$\frac{1}{K^*}\frac{\mathrm{d}N(x)}{\mathrm{d}x} = k_1\int_0^x \frac{N(\xi)}{E_1A_1}\,\mathrm{d}\xi + k_2\int_0^x \frac{N(\xi)}{E_2A_2}\,\mathrm{d}\xi - \alpha_1\Delta T_1 x + \alpha_2\Delta T_2 x \tag{7a}$$

By derivation of the previous relationship and recalling the boundary conditions of Eq. (3), the following second order differential equation can be derived:

$$\begin{aligned} &\frac{\mathrm{d}^2N(x)}{\mathrm{d}x^2} - \alpha^2 N(x) = \beta, \qquad \begin{cases} N(x=-c) = 0 \\ \dfrac{\mathrm{d}N}{\mathrm{d}x}(x=0) = 0 \end{cases} \\ &\alpha^2 = K^*\left(\frac{k_1}{E_1A_1} + \frac{k_2}{E_2A_2}\right), \qquad \beta = K^*(\alpha_2\Delta T_2 - \alpha_1\Delta T_1) \end{aligned} \tag{7b}$$

This differential equation, together with the boundary conditions shown alongside, makes it possible to determine the load, section by section. The solution of equation (7) is

$$N(x) = C_1\mathrm{e}^{\alpha x} + C_2\mathrm{e}^{-\alpha x} - \frac{\beta}{\alpha^2} \tag{8}$$

The constants C_1 and C_2 can be obtained from the boundary conditions as

$$C_1 = C_2 = C = \frac{\beta}{2\alpha^2\cosh(\alpha c)} \tag{9}$$

so that

$$N(x) = \frac{\beta}{\alpha^2}\left(\frac{\cosh(\alpha x)}{\cosh(\alpha c)} - 1\right) \tag{10}$$

Function $N(x)$ being known, we finally can obtain the tangential stress at the interface through Eq. (1), as well as the normal stresses in the two layers. We have to remind that the axial loads are applied at the interface. For a graded layer, the axial stress can be obtained considering the classical theory of multi-layered beams (that assumes the conservation of plane sections) as

$$\sigma(y) = \frac{E(y)}{E_\mathrm{r}}\left(\frac{N}{A^*} + \frac{M}{I^*}y\right) \tag{11}$$

where E_r is a Young's modulus reference value, N, M are respectively the axial load and the bending moment and:

$$A^* = \int_A \frac{E(y)}{E_\mathrm{r}}\,\mathrm{d}A \tag{12}$$

is the *weighted area*, whereas:

$$I^* = \int_A \frac{E(y)}{E_r} y^2 \, dA \tag{13}$$

represents the *weighted moment of inertia*.

The origin of the reference system, from which we have to evaluate y in Eqs. (11) and (13), is defined by the following relationship, defining the *elastic centroid*:

$$S^* = \int_A \frac{E(y)}{E_r} y \, dA = 0 \tag{14}$$

where S^* is the *weighted static moment*.

Let us suppose the graded layer ith, with Young's modulus linearly varying between E_i (value at the interface) and E^i. Applying Eq. (14), we can obtain for each element ($i = 1, 2$) the distance between the origin of the corresponding reference system and the common interface:

$$\bar{y}_i = \frac{h_i E_i + 2h_i E^i}{3(E^i + E_i)} \tag{15}$$

and, from Eqs. (12) and (13):

$$A_i^* = \frac{bh_i}{2E_r}(E^i + E_i) \tag{16}$$

$$I_i^* = \frac{bh_i}{E_r}\left\{E_i\left[\frac{h_i^2}{12} + \frac{\bar{y}_i^2}{2} - \frac{\bar{y}_i h_i}{3}\right] + E^i\left[\frac{h_i^2}{4} + \frac{\bar{y}_i^2}{2} - \frac{2\bar{y}_i h_i}{3}\right]\right\} \tag{17}$$

Introducing Eqs. (16) and (17) into Eq. (11) and considering the common reference system of Fig. 1, gives the stresses in the two elements (constant along the z-axis), that are represented, for the considered example of linear grading, by parabolic functions:

$$\sigma_1(x,y) = \left[\frac{E_1}{E_r} + \left(\frac{E^1}{E_r} - \frac{E_1}{E_r}\right)\frac{(-y)}{h_1}\right]\left(\frac{N(x)}{A_1^*} + \frac{N(x)\bar{y}_1}{I_1^*}(y + \bar{y}_1)\right) \tag{18a}$$

$$\sigma_2(x,y) = \left[\frac{E_2}{E_r} + \left(\frac{E^2}{E_r} - \frac{E_2}{E_r}\right)\left(\frac{y}{h_2}\right)\right]\left(\frac{-N(x)}{A_2^*} + \frac{N(x)\bar{y}_2}{I_2^*}(y - \bar{y}_2)\right) \tag{18b}$$

Evaluating Eqs. (18) at $y = 0$ gives finally the unknowns $k_i \equiv \sigma_i(x, y = 0)A_i/N_i(x)$ as

$$k_i = \frac{E_i}{E_r}\left[\frac{A_i}{A_i^*} + \frac{A_i \bar{y}_i^2}{I_i^*}\right] \tag{19}$$

For the case of non-graded layers ($E_i = E^i$), $k_i = 4$ and Eqs. (18) become:

$$\sigma_1(x,y) = \frac{\beta}{\alpha^2 b h_1}\left(\frac{\cosh(\alpha x)}{\cosh(\alpha c)} - 1\right)\left(1 + 6\left(\frac{y}{h_1} + \frac{1}{2}\right)\right) \tag{20a}$$

$$\sigma_2(x,y) = \frac{\beta}{\alpha^2 b h_2}\left(1 - \frac{\cosh(\alpha x)}{\cosh(\alpha c)}\right)\left(1 + 6\left(\frac{1}{2} - \frac{y}{h_2}\right)\right) \tag{20b}$$

that are linear functions. Obviously, the theory previously presented can be applied to different types of grading.

As a matter of fact, the tangential stress can be obtained from Eq. (1) as

$$\tau(x) = -\frac{\beta \sinh(\alpha x)}{b\alpha \cosh(\alpha c)} \tag{21}$$

The mean value of the tangential stress is zero. Its maximum absolute value is reached at the free ends:

$$\tau_{\max} = |\tau(x = \mp c)| = \frac{|\beta|}{\alpha b}\tanh(\alpha c) \approx \frac{|\beta|}{\alpha b} \tag{22}$$

where the last equality is verified for real mechanical components (e.g., metal cutters), for which αc is of the order of 10.

It is very important to emphasize that the theory predicts a stress-concentration for the interface shearing stresses at the free ends, for any given finite thickness h of the transition zone. On the other hand, a stress-intensification (stresses tending to infinity) appears for vanishing thickness h.

The mean value of the axial load along the x-axis is

$$\langle N(x)\rangle = \frac{1}{2c}\int_{-c}^{+c} N(x)\,\mathrm{d}x = \frac{\beta}{c\alpha^3}\tanh(\alpha c) - \frac{\beta}{\alpha^2} \approx -\frac{\beta}{\alpha^2}\left(\frac{\alpha c - 1}{\alpha c}\right) \approx -\frac{\beta}{\alpha^2} \tag{23}$$

that practically coincides with its maximum value:

$$N_{\max} = N(x = 0) = \frac{\beta}{\alpha^2}\left(\frac{1}{\cosh(\alpha c)} - 1\right) \approx -\frac{\beta}{\alpha^2} \tag{24}$$

This means that the axial load and the normal stresses are substantially constant along the longitudinal axis.

On the other hand, the mean and maximum values for the stresses (18) are:

$$\langle \sigma_i(x)\rangle_y = \frac{N_i(x)}{A_i} \tag{25a}$$

$$\sigma_{i_{\max}}(x) = k_i\langle \sigma_i(x)\rangle_y \tag{25b}$$

$$\sigma_{i_{\max}} = |k_i\langle \sigma_i(x = 0)\rangle_y| = \left|\frac{k_i}{A_i}\frac{\beta}{\alpha^2}\left(\frac{1}{\cosh(\alpha c)} - 1\right)\right| \approx \frac{k_i}{A_i}\frac{|\beta|}{\alpha^2} \tag{25c}$$

The maximum tangential and normal stresses (22) and (25c) act at different points. In any case, the critical condition from a stress viewpoint is reached when the equivalent stress (von Mises, Tresca, et al.) equals its critical value.

It is important to note that the ratio:

$$\bar{s} = \frac{2\tau_{\max}}{\sigma_{\max}} \approx \frac{2h_i^{\min}\alpha}{k_i} \tag{26}$$

with $\sigma_{\max} = \max \sigma_{i_{\max}}$, appears of the order of the unity, so that shearing and normal stresses are competing.

In a multi-layered composite plate under axial load, an additional significant component of the stress tensor is to be considered, besides the tangential and normal stresses previously discussed: this is the shearing stress at the interface along the z-axis. It can be (prudently) estimated considering the deformation imposed by the transversal contraction of the two layers. The transverse displacement at the interface for the ith layer is

$$w_i(x, z) = -\frac{\nu_i k_i N_i(x)}{E_i A_i} z \tag{27}$$

ν_i being the Poisson's ratio at the interface for the ith layer. As a consequence, the shearing stress imposed by the transversal contraction is

$$\tau_\perp(x, z) = \frac{G}{h}\Delta w = \frac{G}{h}(w_2 - w_1) = \frac{G}{h}\frac{\beta}{\alpha^2}\left(\frac{\nu_1 k_1}{E_1 A_1} + \frac{\nu_2 k_2}{E_2 A_2}\right)\left(\frac{\cosh(\alpha x)}{\cosh(\alpha c)} - 1\right) z \tag{28}$$

which, when $v_1 = v_2 = v$, becomes:

$$\tau_{\perp}(x,z) = \frac{\beta v}{b}\left(\frac{\cosh(\alpha x)}{\cosh(\alpha c)} - 1\right) z \tag{29}$$

Its maximum value is

$$\tau_{\perp \max} = \tau_{\perp}\left(x = 0, z = \frac{b}{2}\right) \approx \frac{\beta v}{2} \tag{30}$$

3. Thermal delamination in FGMs

The maximum stresses at the interface could result in a delamination between the two elements, i.e., a brittle crack propagation between dissimilar materials. We will study this phenomenon from an energy viewpoint following the approach proposed by Pugno and Carpinteri (2002, 2003).

By virtue of the energy balance, the following relationship between the variation in the total potential energy $\mathrm{d}W_{\mathrm{therm}}$ due to the thermal load and the fracture energy $\mathsf{G}\mathrm{d}S$ must hold:

$$\mathsf{G}\mathrm{d}S + \mathrm{d}W_{\mathrm{therm}} = 0 \tag{31}$$

where $\mathrm{d}S$ represents the incremental fracture area.

Since the applied load is zero, the variation in the total potential energy due to the thermal load is equal to the variation in the elastic strain energy:

$$\mathrm{d}W_{\mathrm{therm}} = \mathrm{d}L \tag{32}$$

Let us consider that, for imposed mechanical loading, the result is opposite (Pugno and Carpinteri, 2002), i.e.:

$$\mathrm{d}W_{\mathrm{therm}} = -\mathrm{d}W_{\mathrm{mech}} \tag{33}$$

The strain energy release rate can be rewritten as

$$\mathsf{G} = -\frac{\mathrm{d}W_{\mathrm{therm}}}{\mathrm{d}S} = -\frac{\mathrm{d}L}{\mathrm{d}S} \tag{34}$$

Brittle crack propagation, i.e. delamination at the interface in the present case, really occurs when G reaches its critical value G_{F}, characteristic of the interface:

$$\mathsf{G} = -\frac{\mathrm{d}L}{\mathrm{d}S} = \mathsf{G}_{\mathrm{F}} \tag{35}$$

The crack propagation will be stable, metastable or unstable, depending on the sign of the second order derivative of the total potential energy:

$$\frac{\mathrm{d}^2 W_{\mathrm{therm}}}{\mathrm{d}S^2} = -\frac{\mathrm{d}\mathsf{G}}{\mathrm{d}S} = \frac{\mathrm{d}^2 L}{\mathrm{d}S^2} \begin{cases} < 0, & \text{unstable} \\ = 0, & \text{metastable} \\ > 0, & \text{stable} \end{cases} \tag{36}$$

Again, the result is opposite with respect to the imposed mechanical loading (Pugno and Carpinteri, 2002).

To solve the problem of crack propagation, it is necessary to evaluate the elastic strain energy of the FGMS as a function of the crack length. The energy L absorbed by the FGMS is the sum of three quantities, i.e., the elastic strain energy absorbed by the two layers (pedex 1, 2) and by the interface (pedex 3):

$$L = L_1 + L_2 + L_3 \approx L_1 + L_2 \tag{37}$$

the interface being of a very small thickness h.

The elastic strain energy per unit length can be obtained taking into account Eq. (11), as

$$\frac{\mathrm{d}L(x)}{\mathrm{d}x} = \int_A \frac{1}{2}\frac{\sigma^2(y)}{E(y)}\,\mathrm{d}A = \frac{1}{2E_\mathrm{r}}\left(\frac{N^2(x)}{A^*} + \frac{M^2(x)}{I^*}\right) \tag{38}$$

so that, by the definitions in Eqs. (12)–(14), we have:

$$\frac{\mathrm{d}L_i(x)}{\mathrm{d}x} = \frac{k_i N^2(x)}{2E_i A_i} \tag{39}$$

It is very interesting to note that axial load and bending moment remain *energetically orthogonal* also in a graded beam, as derived in Eq. (38).

As previously shown, the shearing stresses of delamination at the interface present their maximum absolute value at the ends of the FGM structure. The initial separation at the interface between the two adherends is supposed to take place at these points: the debonding is represented by two symmetric cracks of length $a/2$. The elastic strain energy of the FGM structure can be evaluated by considering that the axial loads in the two elements are approximately coincident with β/α^2 for a length $2c - a$, and zero outside:

$$\begin{aligned} L &= \int_{-c+a/2}^{c-a/2}\left(\frac{\mathrm{d}L_1(x)}{\mathrm{d}x} + \frac{\mathrm{d}L_2(x)}{\mathrm{d}x}\right)\mathrm{d}x = \int_{-c+a/2}^{c-a/2}\left(\frac{k_1}{2E_1A_1} + \frac{k_2}{2E_2A_2}\right)N^2(x)\,\mathrm{d}x = \frac{\alpha^2}{2K^*}\int_{-c+a/2}^{c-a/2}N^2(x)\,\mathrm{d}x \\ &\cong \frac{\beta^2(c-a/2)}{\alpha^2 K^*} \end{aligned} \tag{40}$$

From Eq. (35) we can obtain the critical value of the parameter β at delamination:

$$\beta_{\mathrm{cr}}^{\mathrm{d}} = \alpha\sqrt{2bK^*\mathsf{G}_\mathrm{F}} \tag{41}$$

and Eq. (36) shows that the crack propagation is metastable:

$$\frac{\mathrm{d}^2L}{\mathrm{d}S^2} = 0 \quad \Rightarrow \quad \text{metastable regime} \tag{42}$$

If we consider $\Delta T_1 = \Delta T_2 = \Delta T$, the critical thermal load becomes:

$$\Delta T_{\mathrm{cr}} = \frac{\beta_{\mathrm{cr}}}{\Delta\alpha K^*} \tag{43}$$

where $\Delta\alpha = |\alpha_2 - \alpha_1|$.

On the other hand, considering a stress criterion at the interface ($\tau_{\max} = \tau_\mathrm{u}$), from Eq. (22) we have:

$$\beta_{\mathrm{cr}}^{\mathrm{u}} \cong \tau_\mathrm{u}\alpha b \tag{44}$$

τ_u being the ultimate shearing stress of the interface. Strength collapse shall precede brittle crack propagation if, and only if, the following dimensionless number will be larger than 1:

$$s = \frac{\beta_{\mathrm{cr}}^{\mathrm{d}}}{\beta_{\mathrm{cr}}^{\mathrm{u}}} = \sqrt{\frac{2G\mathsf{G}_\mathrm{F}}{\tau_\mathrm{u}^2 h}}\begin{cases} > 1 & \tau_{\max} = \tau_\mathrm{u} \\ < 1 & \mathsf{G} = \mathsf{G}_\mathrm{F} \end{cases} \tag{45}$$

From Eq. (35) we can also obtain the stress-intensity factor due to thermal loading. Since

$$\mathsf{G} = \frac{K_I^2}{E'} + \frac{K_{\mathrm{II}}^2}{E'} + \frac{1+\nu}{E}K_{\mathrm{III}}^2 \tag{46}$$

with $E' = E$ for plain stress and $E' = \frac{E}{1-\nu^2}$ for plain strain, in the present case of pure Mode II:

$$K_{\mathrm{II}} = \sqrt{E\mathsf{G}} = \sqrt{-E\frac{\mathrm{d}L}{\mathrm{d}S}} = \beta\sqrt{\frac{E}{2b\alpha^2 K^*}} \tag{47a}$$

which, for $\Delta T_1 = \Delta T_2 = \Delta T$, becomes:

$$K_{\mathrm{II}} = \sqrt{E\mathsf{G}} = \sqrt{-E\frac{\mathrm{d}L}{\mathrm{d}S}} = \Delta\alpha\sqrt{\frac{EK^*}{2b\alpha^2}}\Delta T \tag{47b}$$

This result allows to evaluate the fatigue life during thermal cycles by using the well-known Paris' law. Assuming to replace the stress-intensity factor in Mode I with its equivalent value, which here coincides with the stress-intensity factor in Mode II:

$$\frac{\mathrm{d}a}{\mathrm{dN}} = C(\Delta K)^m \tag{48}$$

with $N =$ number of cycles; $\Delta K = K_{\mathrm{II}}(\max) - K_{\mathrm{II}}(\min) =$ variation in the (equivalent) stress-intensity factor due to the variation in the thermal load ΔT; C, m Paris' constants. Eq. (47b) exhibits a value of the stress-intensity factor independent of a. The fatigue life of the FGMS due to thermal cycles can be estimated simply by integration of Eq. (48):

$$N_{\mathrm{TOT}} = \int_0^{N_{\mathrm{TOT}}} \mathrm{d}N = \int_{a_0}^{2c} \frac{\mathrm{d}a}{C(\Delta K_{\mathrm{II}})^m} = \frac{2c - a_0}{C\left(\Delta\alpha\sqrt{\frac{EK^*}{2b\alpha^2}}(\Delta T(\max) - \Delta T(\min))\right)^m} \tag{49}$$

4. Example of application

As an example, we analyse in this section a hard metal cutter composed by two layers (hard cutting layer and metal substrate), for which we assume the following reasonable parameters (see Lammer, 1988; Huang et al., 1997):

$$E_1 = 4.7\times10^{11}\ \mathrm{Pa};\quad E_2 = 8.3\times10^{11}\ \mathrm{Pa};\quad G \approx \frac{E}{2} = \frac{E_1+E_2}{4} = 3.25\times10^{11}\ \mathrm{Pa};$$
$$h_1 = 10^{-2}\ \mathrm{m};\quad h_2 = 10^{-3}\ \mathrm{m};\quad h \approx 10^{-4}\ \mathrm{m};\quad b = 3\times10^{-3}\ \mathrm{m};\quad c = 5.5\times10^{-3}\ \mathrm{m};$$
$$(A_1 = bh_1,\ A_2 = bh_2);$$
$$\alpha_1 = 5.2\times10^{-6}\ ^\circ\mathrm{C}^{-1};\quad \alpha_2 = 2.23\times10^{-6}\ ^\circ\mathrm{C}^{-1};\quad \tau_{\mathrm{u}} = 10^9\ \mathrm{Pa};$$
$$K_{\mathrm{IC1}} = 30\times10^6\ \mathrm{Pa}\sqrt{\mathrm{m}};\quad K_{\mathrm{IC2}} = 10.5\times10^6\ \mathrm{Pa}\sqrt{\mathrm{m}};\quad \mathsf{G}_{\mathrm{F}} = \frac{K_{\mathrm{IC}}^2}{E} \approx \frac{(K_{\mathrm{IC1}}+K_{\mathrm{IC2}})^2}{4E} = 615\ \mathrm{N/m}.$$

Applying Eqs. (41), (43) and (44), the tangential strength limit condition is predicted when $\Delta T_{\mathrm{cr}}^{\mathrm{u}} = 444\ ^\circ\mathrm{C}$, before delamination, which is expected for $\Delta T_{\mathrm{cr}}^{\mathrm{d}} = 888\ ^\circ\mathrm{C}$. In addition, shearing stresses prevail over normal ones ($\bar{s} = 2.07$, from Eq. (26)).

If we consider $\mathsf{G}_{\mathrm{F}} = \min\{\mathsf{G}_{\mathrm{F1}}, \mathsf{G}_{\mathrm{F2}}\} = 120\ \mathrm{N/m}$ (fracture in the brittler layer rather than at the interface), we obtain $\Delta T_{\mathrm{cr}}^{\mathrm{d}} = 443\ ^\circ\mathrm{C}$, so that tangential strength overcoming and debonding are competing failure mechanisms.

The axial load and the tangential stress along the x-axis are respectively reported in Figs. 2–4 for the case $\Delta T_1 = \Delta T_2 = 500\ ^\circ\mathrm{C}$, as well as the stress in the cutter along the y-axis in the critical section ($x = 0$). The stresses are found to be tremendously high for working temperatures of a few hundreds Celsius degrees.

In Fig. 5a and b, the equivalent Tresca's stresses are reported along the x-axis at the interface (critical section, $y = 0$), respectively on cutting layer (a) and on substrate (b). The strength collapse of the cutter arises at the free ends of substrate (lower strength) and it is due to tangential stresses.

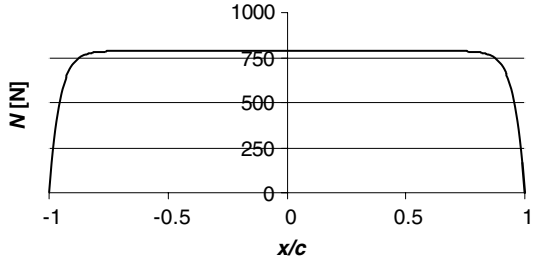

Fig. 2. Axial load.

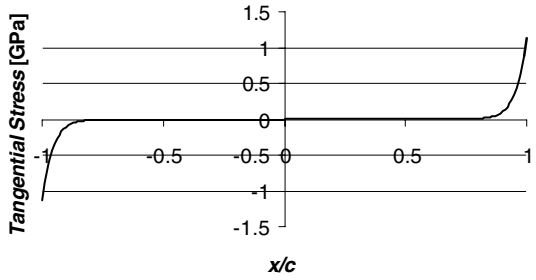

Fig. 3. Tangential stress.

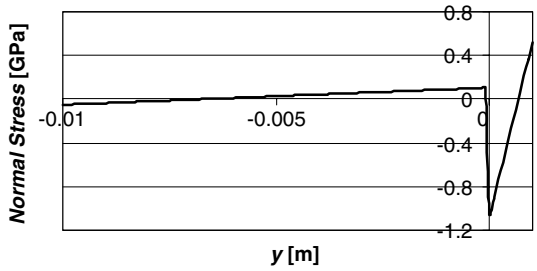

Fig. 4. Normal stress.

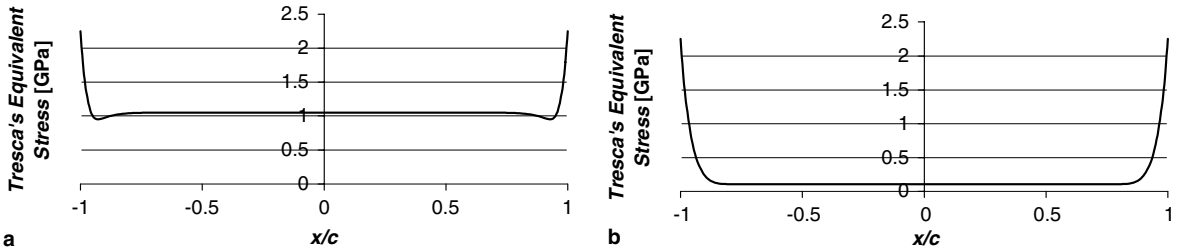

Fig. 5. (a) Tresca equivalent stress on cutting layer. (b) Tresca equivalent stress on substrate.

The value $\tau_{\perp\max} \approx \frac{\nu\beta}{2}$, assuming $\nu \approx 0.2$, is equal to 1.45 GPa, which is comparable, as expected, with the other maximum stresses.

The estimation of the fatigue life for the cutter can be obtained considering the Paris' constants C and m. Their typical values for metals are $m = 1$–4 and $C \approx 1-3 \times 10^{-15}$ (SI). For example, in cutting reinforced concrete, the cutter presents different temperatures when it is in the metal or in concrete. The frequency of the impacts against the re-bar, as well as the frequency of the thermal load, is of the order of 10 Hz. The difference in the temperatures is of the order of 20 °C (total value around 300 °C). Introducing in Eq. (49) $\Delta T\ (\max) - \Delta T\ (\min) \approx 20$ °C and $a_0 \approx 0$, we obtain a fatigue life prediction of $N_{\mathrm{TOT}} \cong 8.5 \times 10^6$ cycles ($m = 1$, $C \approx 2.875 \times 10^{-15}$ in SI).

5. Shape/size effects and optimization

From the previous formulas, the influence of the geometrical parameters on the strength of the element, as well as the related shape and size effects, can be derived. The maximum shearing stress is

$$\tau_{\max} \approx \frac{\sqrt{G}(\alpha_2 \Delta T_2 - \alpha_1 \Delta T_1) b}{2\sqrt{\frac{1}{E_1}\frac{h}{h_1} + \frac{1}{E_2}\frac{h}{h_2}}} \tag{50}$$

The influences of the different geometrical parameters are described in Fig. 6. R is the size of self-similar FGMS: i.e., $h_1 \propto h_2 \propto b \propto h \propto R$; r is the size of quasi-self-similar FGMS: i.e., $h_1 \propto h_2 \propto b \propto r$, in which we consider $h =$ constant, since it represents a parameter imposed by the chemistry of the bonding rather than a free design parameter. The maximum shearing stress tends to vanish when the structural size decreases. The tangential stress of Eq. (50) tends to infinity when the thickness of the transition zone goes to zero; on the other hand, it tends to zero reducing the size of the cutter, see Fig. 6.

The maximum normal stresses are:

$$\sigma_{\max 1} \approx \frac{(\alpha_2 \Delta T_2 - \alpha_1 \Delta T_1)}{\sqrt{\frac{1}{E_1} + \frac{1}{E_2}\frac{h_1}{h_2}}}, \qquad \sigma_{\max 2} \approx \frac{(\alpha_2 \Delta T_2 - \alpha_1 \Delta T_1)}{\sqrt{\frac{1}{E_2} + \frac{1}{E_1}\frac{h_2}{h_1}}} \tag{51}$$

The influences of the different geometrical parameters are described in Fig. 7. Differently from the previous case, the normal stresses are independent of the size-scale R. We cannot reduce the normal stresses simply by a reduction of the structural size. On the other hand, we could reduce them by an optimization of the ratio h_1/h_2. The optimal value for the ratio h_1/h_2 is reported in Fig. 7 imposing $\sigma_{\max 1} = \sigma_{\max 2}$.

A better optimization could be obtained considering the different strengths of the two layers and by imposing the following condition:

$$\frac{\sigma_{\max 1}}{\sigma_{\mathrm{u}1}} = \frac{\sigma_{\max 2}}{\sigma_{\mathrm{u}2}} \tag{52}$$

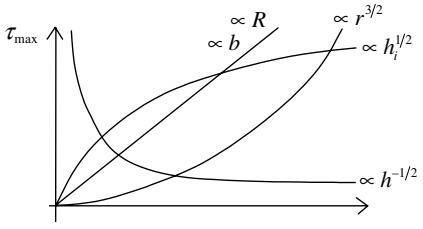

Fig. 6. Influence of geometry on maximum shearing stress.

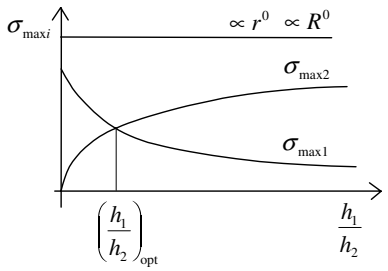

Fig. 7. Influence of geometry on maximum normal stresses.

Eq. (52) can be rewritten as

$$\frac{\sigma_{u1}}{E_2}\left(\frac{h_1}{h_2}\right)^2+\left(\frac{\sigma_{u1}}{E_1}-\frac{\sigma_{u2}}{E_2}\right)\left(\frac{h_1}{h_2}\right)-\frac{\sigma_{u2}}{E_1}=0 \tag{53}$$

and gives two solutions for the optimal ratio h_1/h_2. One of them is unacceptable (<0), whereas the other is

$$\left(\frac{h_1}{h_2}\right)_{opt}=\frac{\sigma_{u2}}{\sigma_{u1}} \tag{54}$$

This result allows to optimize the ratio h_1/h_2 between substrate and cutting layer of the tool. From a thermal stress viewpoint, the best solution should imply considering also layers with functional graded materials, to reduce the mismatch of the thermal expansion coefficients. Assuming $\sigma_{max2}>\sigma_{max1}$ (cutting layer with higher stresses), the gain λ related to this optimization is

$$\lambda=\frac{\sigma_{max\,2}}{\sigma_{max\,2}(opt)}\approx\frac{\sqrt{1+\frac{E_2}{E_1}\left(\frac{h_2}{h_1}\right)_{opt}}}{\sqrt{1+\frac{E_2}{E_1}\frac{h_2}{h_1}}} \tag{55}$$

For example, assuming for a metal cutter $E_2\approx 2E_1$ and $h_1\approx 4h_2$, so that $\lambda\approx 1.25$, which means that the optimization could provide an increment in the cutter's strength by 25%.

In addition, the maximum orthogonal shearing stress is

$$\tau_{\perp max}\approx\sqrt{G}(\alpha_2\Delta T_2-\alpha_1\Delta T_1)\sqrt{\frac{b}{h}} \tag{56}$$

The influences of the different geometrical parameters on the shearing stress of Eq. (56) are described in Fig. 8. R is the size of self-similar cutters. For quasi-self-similar cutters (constant interface thickness), smaller is stronger, whereas for completely self-similar cutters the influence of the size disappears.

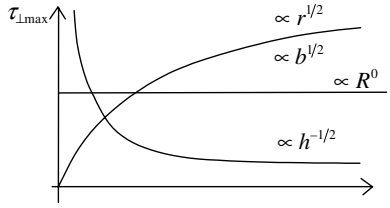

Fig. 8. Influence of geometry on maximum orthogonal shearing stress.

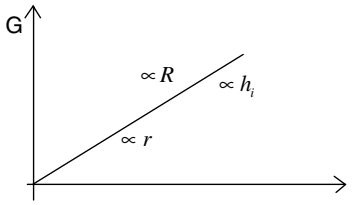

Fig. 9. Influence of geometry on energy release rate.

Finally, for the energy release rate we have:

$$\mathsf{G} \approx \frac{\sqrt{G}(\alpha_2 \Delta T_2 - \alpha_1 \Delta T_1)^2}{8\left(\frac{1}{E_1 h_1} + \frac{1}{E_2 h_2}\right)} \tag{57}$$

The brittle crack propagation will arise when $\mathsf{G} = \mathsf{G}_\mathrm{F}$. The influences of the different geometrical parameters are described in Fig. 9. G decreases by considering smaller cutters, so that smaller is stronger also from a brittle crack propagation viewpoint.

6. Conclusions

The stress field and the fracture propagation conditions due to thermal loading in multi-layered and/or functionally graded materials have been analysed. The shearing stress field at the interface, as well as the normal stresses in the layers, have been computed. The delamination phenomenon between the layers has been predicted by a fracture mechanics analysis. The findings allow to estimate the critical temperature corresponding to limit strength or brittle fracture, of great importance in the design of innovative components in high temperature environment. The influences of the geometrical parameters, describing the so called shape- and size-effects, have been also discussed. An application to the interesting case of metal cutters concludes the paper. Even if numerical simulations in both static (Pugno and Surace, 2000) and dynamic (Pugno and Ruotolo, 2002) regimes as well as experimental observations (Pugno and Carpinteri, 2002) have already confirmed—for homogeneous structures—the general approach here presented, numerical investigations for functionally graded material structures will be presented in a future paper.

References

Atkinson, C., List, R.D., 1978. Steady state crack propagation into media with spatially varying elastic properties. Int J. Eng. Sci. 16, 717–730.

Babaei, R., Lukasiewicz, S.A., 1998. Dynamic response of a crack in a functionally graded material between two dissimilar half-planes under anti-plane shear impact load. Eng. Fract. Mech. 60, 479–487.

Carpinteri, A., Pugno, N., 2005. Fracture instability and limit strength condition in structures with re-entrant corners. Eng. Fract. Mech. 72, 1254–1267.

Carpinteri, A., Paggi, M., Pugno, N., in press. Numerical evaluation of generalized stress-intensity factors in multi-layered composites. Int. J. Sol. Struct., doi:10.1016/j.ijsolstr.2005.06.009.

Delale, F., Erdogan, F., 1983. The crack problem for a nonhomogeneous plane. J. Appl. Mech. 50, 609–614.

Eischen, J.W., 1987. Fracture of nonhomogeneous materials. Int. J. Fract. 34, 3–22.

Erdogan, F., 1995. Fracture mechanics of functionally graded materials. Compos. Eng. 7, 753–770.

Erdogan, F., Wu, B.H., 1996. Crack problems in FGM layers under thermal stresses. J. Therm. Stresses 19, 237–265.

Huang, B.-L., Weis, C., Yao, X., Belnap, D., Rai, G., 1997. Fracture toughness of sintered polycrystalline diamond (PCD). In: Froes, F.H., Hebeisen, J.C. (Eds.), Proceedings of the 5th International Conference on Advanced Particulate Materials and Processes. Metal Powder Industries Federation, Princeton, NJ, pp. 431–437.

Jin, Z.H., Noda, N., 1993. An internal crack parallel to the boundary of a nonhomogeneous half plane under thermal loading. Int. J. Eng. Sci. 31, 793–806.
Jin, Z.H., Batra, R.C., 1996. Stress intensity relaxation at the tip of an edge crack in a functionally graded material subjected to a thermal shock. J. Therm. Stresses 19, 317–339.
Jin, Z.H, Paulino, G.H., 2001. Transient thermal stress analysis of an edge crack in a functionally graded material. Int. J. Fract. 107, 73–98.
Lammer, A., 1988. Mechanical properties of polycrystalline diamonds. Mater. Sci. Tech. 4, 949–955.
Ozturk, M., Erdogan, F., 1997. Mode I crack problem in an inhomogeneous orthotropic medium. Int. J. Eng. Sci. 35, 869–883.
Ozturk, M., Erdogan, F., 1999. The mixed mode crack problem in an inhomogeneous orthotropic medium. Int. J. Fract. 98, 243–261.
Parameswaran, V., Shukla, A., 1998. Dynamic fracture of a functionally gradient material having discrete property variation. J. Mater. Sci. 33, 3303–3311.
Paulino, G.H. (Guest ed.), 2002. On fracture of functionally graded materials. Eng. Fract. Mech. 69 1519–1809
Pugno, N., 1999. Optimising a non-tubular adhesive bonded joint for uniform torsional strength. Int. J. Mater. Product Technol. 14, 476–487.
Pugno, N., 2001. Closed form solution for a non-tubular bonded joint with tapered adherends under torsion. Int. J. Mech. Control 2, 19–27.
Pugno, N., Carpinteri, A., 2002. Strength, stability and size effects in the brittle behaviour of bonded joints under torsion: theory and experimental assessment. Fatigue Frac. Eng. Mater. Struct. 25, 55–62.
Pugno, N., Carpinteri, A., 2003. Tubular adhesive joints under axial load. J. Appl. Mech. 70, 832–839.
Pugno, N., Ruotolo, R., 2002. Evaluation of torsional natural frequencies for non-tubular bonded joints. Struct. Eng. Mech. 13, 91–101.
Pugno, N., Surace, G., 2000. Non-tubular bonded joint under torsion: theory and numerical validation. Struct. Eng. Mech. 10, 125–138.
Pugno, N., Surace, G., 2001. Tubular bonded joint under torsion: analysis and optimization for uniform torsional strength. J. Strain Anal. Eng. Design 1, 17–24.
Wang, B.L., Han, J.C., Du, S.Y., 2000. Crack problems for functionally graded materials under transient thermal loading. J. Therm. Stresses 23, 143–168.
Wang, B.L., Noda, N., 2001. Thermally induced fracture of a smart functionally graded composite structure. Theor. Appl. Fract. Mech. 35, 93–109.